Atmospheric Environment 334 (2024) 120708

Contents lists available at ScienceDirect

Atmospheric Environment

journal homepage: www.elsevier.com/locate/atmosenv

Region-oriented simultaneously joint two-pollutant control strategies are required to substantially reduce deaths attributed to both $PM_{2.5}$ and ozone pollution in China

Baozhang Chen [a,b,c,*], Sheng Zhong [d,e,**], Nicholas A.S. Hamm [f], Hong Liao [g], Tong Zhu [h], Shu'an Liu [a], Huifang Zhang [b,c], Lifeng Guo [b], Kun Hou [a]

[a] School of Remote Sensing and Geomatics Engineering, Nanjing University of Information Science and Technology, Nanjing, 210044, China
[b] State Key Laboratory of Resource and Environmental Information System, Institute of Geographic Sciences and Natural Resources Research, Chinese Academy of Sciences, Beijing, 100101, China
[c] University of Chinese Academy of Sciences, Beijing, China
[d] Jiangsu Provincial Environmental Monitoring Center, Nanjing, 210019, China
[e] Jiangsu Collaborative Innovation Center of Atmospheric Environment and Equipment Technology (CICAEET), Nanjing, 210044, China
[f] Geospatial and Geohazards Research Group and School of Geographical Sciences, Faculty of Science and Engineering, University of Nottingham, Ningbo, 315100, China
[g] Jiangsu Key Laboratory of Atmospheric Environment Monitoring and Pollution Control, Collaborative Innovation Center of Atmospheric Environment and Equipment Technology, School of Environmental Science and Engineering, Nanjing University of Information Science and Technology, Nanjing, 210044, China
[h] College of Environmental Sciences and Engineering, Peking University, Beijing, 100871, China

HIGHLIGHTS

- $PM_{2.5}$ targeted policy led a reduction in $PM_{2.5}$ and $PM_{2.5}$-attributable deaths.
- Meanwhile O_3 and O_3-attributable deaths significantly increased.
- Our results indicate that trade-offs may occur in the controls of ozone or $PM_{2.5}$.
- A deep understanding of the chemical reaction is needed between the two pollutants.
- A region-oriented smarter air pollution strategy is required to reduce pollution.

GRAPHICAL ABSTRACT

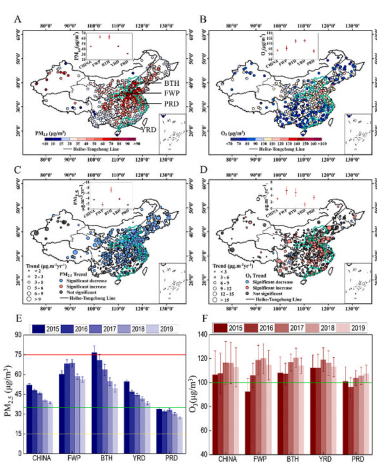

* Corresponding author. School of Remote Sensing and Geomatics Engineering, Nanjing University of Information Science and Technology, Nanjing, 210044, China.

** Corresponding author. Jiangsu Collaborative Innovation Center of Atmospheric Environment and Equipment Technology (CICAEET), Nanjing, 210044, China.

E-mail addresses: baozhang.chen@nuist.edu.cn (B. Chen), zhongs@jshb.gov.cn (S. Zhong).

https://doi.org/10.1016/j.atmosenv.2024.120708
Received 27 October 2023; Received in revised form 13 July 2024; Accepted 18 July 2024
Available online 19 July 2024

ARTICLE INFO

Keywords:
$PM_{2.5}$ and ozone pollution
Ozone and particulate attributed deaths
Region-oriented policy
China

ABSTRACT

China is confronting serious air pollution of fine particulate matter ($PM_{2.5}$) and ozone, which routinely exceed air quality standards. $PM_{2.5}$ concentrations decreased by 30–40% while ozone increased by 15–20%, across China during 2015–2019. This could be attributed to targeted clean air policies that have focused more on controlling particulate matter since 2013. The deaths attributable to $PM_{2.5}$ and ozone exposure over China changed from 1.45 to 0.13 million in 2015 to 1.04 and 0.21 million in 2019, respectively. The changes in mortality, $PM_{2.5}$ and ozone present spatially heterogeneous patterns across cities and regions. The ozone production regimes (NO_x -limited, volatile organic compounds (VOCs)-limited or transition between them), the responses of $P(O_3)$ to the change in NO_x and VOCs, the reactions of HO_2, OH, and RO_2, and meteorological conditions, are regionally dependent and spatially heterogeneous. Our results have important implications for developing a smarter, region-oriented, two-pollutant coordinated control policy for VOCs and NO_x in China.

1. Introduction

Outdoor air pollution has adverse health impacts, as reported by many studies. More than 90% of the world's population lives in places where air pollution concentrations exceed World Health Organization (WHO) guidelines (Zou et al., 2020). Epidemiological research has documented that exposure to hazardous air pollution leads to an increase in in mortality and morbidity and contributes to the global disease burden of respiratory disease, cardiovascular disease and lung cancer(Beelen et al., 2014; Bell et al., 2004; Brook et al., 2010; Hoek et al., 2013; Jerrett et al., 2009). According to the Global Burden of Disease project report, outdoor air pollution is one of the top five risk factors worldwide, causing approximately 4 million deaths in 2017 (Stanaway et al., 2018), accounting for one-ninth of the total global mortality(Yue et al., 2020a). About 1 million premature death each year are caused by air pollution in China (Shen et al., 2017).

There are numerous air pollutants cause hazardous health outcomes, including particles such as fine particulate matter with an aerodynamic diameter less than 2.5 μm ($PM_{2.5}$) and ozone (O_3) (Burns et al., 2020). These two pollutants were selected as indicators in the Global Burden of Disease studies due to their significant health impacts supported by scientific research and a clear exposure-response relationship, which facilitates their quantification, despite remaining uncertainties in assessing their health impacts.

Ambient $PM_{2.5}$ pollution, which contributes to various respiratory and cardiovascular diseases(Yue et al., 2020a), is the greatest environmental risk factor for human health globally (Burns et al., 2020; Y. Zhou et al., 2020). Surface level ozone also induces respiratory problems and increases morbidity and mortality via impairment of lung functions (Hao et al., 2015; Zhong et al., 2019).

Ambient air pollution has become one of the most severe environmental and health issues in China, with $PM_{2.5}$ and surface ozone routinely exceeding air quality standards (Burns et al., 2020; Fan et al., 2020a,b; K. Li et al., 2019; L. Li et al., 2018; R. Li et al., 2015; Lu et al., 2018; Xiao et al., 2020; K. Zhang et al., 2020; Y. Zhou et al., 2020). To mitigate this serious issue, the State Council of China promulgated the toughest-ever Air Pollution Prevention and Control Action Plan (hereafter the Action Plan) in September 2013 (23). As the first national strategy on air pollution control and a milestone, the Action Plan focused principally on controls of $PM_{2.5}$ and in three key regions, i.e., the Beijing-Tianjin-Hebei (BTH) area, the Yangtze River Delta (YRD), and the Pearl River Delta (PRD) (Feng et al., 2019) (Fig.S1). At the same time, the Chinese government has also established other measures and regulations to mitigate the serious levels of air pollution, including the 10 measures for the prevention and control of air pollution from China's State Council in 2013 and the Law of the People's Republic of China on the Prevention Control of Atmosphere Pollution amended in 2015 (Zou et al., 2020). At the National Health Conference in 2016, Chinese President Xi emphasized lifelong health services and China's State Council released the 'Healthy China (2030) Outline' in 2016 (Q. Zhang et al., 2019).

Since 2013, China has implemented a series of policies to control various pollutants, including primary particles, SO_2, NOx, VOCs, NH_3, etc.(K. Chen et al., 2021; Xiao et al., 2020; Q. Zhang et al., 2019). As a result, $PM_{2.5}$ and related health benefits from 2013 to 2017 in China were improved substantially (Silver et al., 2018). However, surface ozone concentrations continued to increase (Lu et al., 2018) and associated mortality also increased (Burns et al., 2020; Kuerban et al., 2020; Malley et al., 2017; Zhong et al., 2019).

Air $PM_{2.5}$ can result from either direct emission or from atmospheric reactions. Tropospheric ozone is produced by photochemical oxidation of volatile organic compounds (VOCs) and CO in the presence of nitrogen oxides ($NO_x \equiv NO + NO_2$) catalyzed by hydrogen oxide radicals ($HO_x \equiv OH + HO_2$) and organic peroxyl radicals (RO_2) (30–31). Many have researchers reported that the secondary compounds of $PM_{2.5}$ can constitute up to 70% of the total concentration in metropolitan cities in China, especially during extreme pollution events (An et al., 2019). The relationships between ozone and its shared precursors with $PM_{2.5}$ (e.g., NO_x and VOCs) are highly nonlinear and complex. In China, during 2013–2017, the bulk $PM_{2.5}$ concentrations and NO_x emissions in China decreased by 30–40% and 20%, respectively, while there were counterproductive effects on ozone (K. Li et al., 2019). Decreases in bulk $PM_{2.5}$ could further affect O_3 formation regimes between NO_x -limited and VOC-limited, while also changing photolysis rates and aerosol chemistry (K. Li et al., 2019; Lu et al., 2019). Therefore, it is impossible to straightforwardly mitigate ozone pollution by simply reducing the emissions of primary pollutants because of the complexity of O_3-$PM_{2.5}$ relationship and O_3-NOx -VOC regime (Tan et al., 2018) and its regionally-dependent sensitivities. In order to get both $PM_{2.5}$ and ozone levels under control, sophisticated and location related regulations of emission reduction may be needed.

Although many studies have investigated the impact, formation, and sources of $PM_{2.5}$ and O_3 pollution in the past few years (An et al., 2019; Fan et al., 2021; Hao et al., 2015; Lu et al., 2019; P. Wang et al., 2020; Q. Zhang et al., 2019), there has been a lack of comparative and comprehensive research on spatiotemporal patterns of both O_3 and $PM_{2.5}$ and their health impacts in China. Given that China is currently plagued by complex O_3 pollution problems, understanding the O_3-$PM_{2.5}$ relationship is of great significance for drafting appropriate regional strategies for efficient control both O_3 and $PM_{2.5}$ pollutants and their health issues. The aim of this study is to improve comprehensive understanding of the regional trends of paired O_3-$PM_{2.5}$ air pollution and their associated human health impacts during 2015–2019 using a large dataset from 1497 surface monitoring sites across China (Fig. S1).

2. Materials and Methods

2.1. Study setting

Six regions are highlighted in this study and are illustrated in Fig. S1 and Table S3. The first phase of the implementation of the Action Plan focused particularly on the three key regions (i.e., BTH, YRD and PRD).

To address severe air pollution issues and protect public health, concentration reductions of 25% (BTH), 20% (YRD), and 15% (PRD) in 2017 compared to the level in 2013 were mandated in these three key regions(Q. Zhang et al., 2019). There is also an urgent need to make a regional joint prevention and control strategy for the Fen-Wei Plain (FWP) and similar areas, which suffer from serious compound pollution (Fan et al., 2020a,b). The Heihe-Tengchong Line (Fig. S1) serves as the delimitation line of population aggregation in China (M. Chen et al., 2016). The area to the southeast of this line is more densely populated (EMPC: Eastern More-populated Part of the Country): 94% of the population lives on 43% of the land area, with population density of 325.84 people/km^2. The area to the northwest of the Heihe-Tenchong Line is sparsely populated (WLPC: Western Less-populated Part of the Country), with a density of 14.68 people/km^2. This pattern is not expected to change (M. Chen et al., 2016) in the coming years.

In this study, we analyzed $PM_{2.5}$ and O_3 associated mortality data for all 367 cities of 31 provinces in mainland China, and highlighted the above mentioned 6 cluster regions (BTH, YRD, PRD, FWP, EMPC and WLPC, fig. S1 and table S3), representing various socio-economic, climatic, air pollution exposure and prevention strategies.

2.2. p.m.$_{2.5}$ and O_3 concentration data

The hourly concentrations of 6 air pollutants including $PM_{2.5}$ and O_3, were measured at 1497 sites during January 1, 2015 to December 31, 2019 in 367 cities and counties, acquired from the national air quality monitoring network operated by China National Environmental Monitoring Center (CNEMC) (https://quotsoft.net/air/). The location of all 1497 monitoring sites is shown in fig. S1. For detailed description of the monitoring instruments, sampling methods and data quality control, see the Supplementary Materials.

2.3. Calculations of daily, monthly, seasonal, and annual mean concentrations of O_3 and $PM_{2.5}$

2.3.1. Data screening and gap filling

Consecutive repeats and zeroes were removed from the hourly time series data. Gaps less than 2 consecutive observations were filled using linear interpolation. Time series with less than 10% of data available were removed. Data were flagged if the daily mean had a low coefficient of variation in a certain period, the site was removed if the number of flagged days is more than 60. The QAQC (data quality assurance and quality control) and data screening procedures are described in detail in ref. (Kuerban et al., 2020; Silver et al., 2018). The number of available sites after QAQC and data screening is 1405 out of 1497 across China.

2.3.2. Maximum daily 8-h moving average O_3 (MDA8 O_3)

The World Health Organization (WHO) set a guideline of 100 μg m^{-3} for a maximum daily 8-h moving average (MDA8) exposure to surface O_3(Organization, 2006). The MDA8 O_3 concentrations were calculated when 5-h or longer non-zero moving averages were available during a given 8-h period, otherwise, the 8-h average was marked as 'missing' value. The 'missing' values was not used in the subsequent analysis. Finally, the maximum daily value of the 8-h moving averages was treated as the valid MDA8 O_3value to represent the O_3 level of that day.

The maximum value of the averaged ozone value of 8 consecutive hours should be taken. For example, $N1 = (c1, c2, c3, \ldots, c8)$, $N2 = (c2, c2, c3, \ldots, c9)$, $N3 = (c3, c2, c3, \ldots, c10)$, and so on, $N17 = (c17, c2, c3, \ldots, c24)$. The maximum value of ozone in 8 h per day, the MDA8 O_3 = $\max(N1, N2, N3, \ldots, N17)$.

2.4. Daily mean concentrations of the five air pollutants (PM_{10}, $PM_{2.5}$, SO_2, NO_2, and CO)

The daily mean concentration at each monitoring site was computed from the hourly time series data, and was calculated as:

$$C_{\mathrm{d}}^{i} = \frac{1}{23}\sum_{\mathrm{t}=0}^{23} \mathrm{h}_{\mathrm{t}}^{i} \tag{1}$$

where C_{d}^{i} and h_{d}^{i} are the daily mean and hourly concentration of a single air pollutant, respectively, t is the hour of day ranging from 0 to 23, i is the investigated air pollutant.

2.5. Monthly, seasonal, and annual mean concentrations of six air pollutants

Monthly concentration of an air pollutant at each site was calculated as:

$$C_{m}^{i} = \frac{1}{\mathrm{p}}\sum_{\mathrm{j}=1}^{\mathrm{p}} \mathrm{C}_{d,j}^{i} \tag{2}$$

where $C_m{}^i$ and C_{dj}^{i} are monthly and daily mean concentration of an individual air pollutant, respectively, j is the day of the month, p is the total number of days for a given calendar month j, and i is the investigated air pollutant.

The months for different seasons were defined as: spring (March–May), summer (June–August), fall (September–November) and winter (December–February). The seasonal or annual concentrations of the investigated air pollutant were calculated from monthly values as:

$$C_{s,a}^{i} = \frac{1}{\mathrm{n}}\sum_{\mathrm{k}=1}^{\mathrm{n}} \mathrm{C}_{m,k}^{i} \tag{3}$$

where $C_{s,a}^{i}$ is the seasonal (subscript s) or annual (subscript a) mean concentrations of an individual air pollutant, $C_{m,k}^{i}$ is the monthly mean concentration of an individual air pollutant for month k, $n = 3$ for seasonal and $n = 12$ for annual calculation, and i is the investigated air pollutant.

2.6. The anthropogenic emission data

Anthropogenic emissions were estimated using the bottom-up inventory model of Multi-resolution Emission Inventory for China (MEIC), developed by Tsinghua University (available at: http://www.meicmodel.org/)(Zheng et al., 2018). MEIC is a widely used bottom-up emission inventory framework that follows a technology-based methodology to calculate emissions from more than 700 anthropogenic source types in China. The annual MEIC data at a 0.25° resolution during 2012–2017 were used to provide the baseline emission and to conduct a measure-by-measure evaluation of emission abatements (K. Li et al., 2019).

2.7. Population and mortality data

We estimated the deaths attributable to $PM_{2.5}$ and O_3 exposures at a city level, covering 31 provinces and 367 cities. The annual average population data during 2015–2019 were acquired from the China Statistical Yearbook (M. Chen et al., 2016) (http://www.stats.gov.cn/english/). The city-level age-specific census data were acquired from the Sixth National Population Census carried out in 2010. The city-level proportions of different age groups during the study period were estimated on the basis of the population growth rate and aging trends of China reported by the United Nation (M. Chen et al., 2016; Nations, 2018). This estimation uncertainty was proved to be relatively small because population growth was slow (J. Huang et al., 2018).

The mortality data were acquired from the Chinese Centers for Disease Control and Prevention (China CDC), which has established 161 death surveillance points since 2004 (J. Huang et al., 2018). The estimates of the deaths attributable to air pollution at a city-level should ideally use city-level baseline mortality data. However, these data are not available in China so we instead used provincial-level data. The proportions of cause-specific mortality in different provinces and age groups were obtained from the China Death Surveillance Dataset in 2013(J. Huang et al., 2018). The baseline respiratory and cardiovascular disease-related mortality rate data were acquired from the Global Burden of Disease (GBD) study in 2016 (http://vizhub.healthdata.org/gbd-compare) (Maji et al., 2019). The age-specific and cause-specific mortality rate for each disease were estimated based on these death surveillance points in 2016 obtained from reports (Q. Wang et al., 2018; M. Zhou et al., 2016) and the results of GBD studies in 2016 (Nichols et al., 2019; Zunt et al., 2018).

2.8. Estimating all-cause deaths attributable to $PM_{2.5}$ and O_3 exposure

Six kinds of diseases related to $PM_{2.5}$ pollution including lung cancer, chronic obstructive pulmonary disease, lower respiratory infection, ischemic heart disease, stroke, and diabetes mellitus type 2, and two kinds diseases of respiratory and cardiovascular disease associated with O_3 were considered in this study.

The cause-specific integrated exposure–response functions have been developed for the GBD studies (Apte et al., 2015; R. T. Burnett et al., 2014; Cohen et al., 2017; Collaborators, 2016; Feigin and Collaborators, 2018; Nichols et al., 2019). Recently, Luben et al. (2018) studied multipollutant effects on cardiovascular disease, while Wang et al. (C. Wang et al., 2023) explored the effect of co-exposure to multiple air pollutants and meteorological conditions on mental health outcomes. These studies provide evidence of synergistic effects from co-exposure to multiple air pollutants, but further research is needed to develop quantification methods for these effects. Wu et al. (2021) employed novel exposure-response functions with multiple exposure windows to estimate the mortality burden attributable to long-term ambient $PM_{2.5}$ exposure in China, revealing significantly higher estimates of premature deaths compared to those obtained using cause-specific integrated exposure–response functions (Wu et al., 2021).

In this study, the all-cause premature deaths attributable to $PM_{2.5}$ and O_3 exposure were estimated using the comparative risk assessment framework (Murray et al., 2003) and a set of epidemiological concentration–response (C–R) functions (Anenberg et al., 2010; Apte et al., 2015; J. Huang et al., 2018; Kuerban et al., 2020; J. Lelieveld et al., 2013; K. Li et al., 2019; Maji et al., 2019; Song et al., 2016), by applying the location-specific and age-specific population-attributable fraction to the number of deaths. Fifteen age groups were included in the equation, i.e., 25–30, 30–35, …,90–95, and beyond 95 years old. For lower respiratory infection, children less than 5 years old were also considered.

The number of annual premature deaths $D_{i,j}$ of disease j attributable to ambient $PM_{2.5}$ or MDA8 O_3 for city i located in region k (i.e., province) were calculated using the following equations (e.g., Anenberg et al., 2010; J. Huang et al., 2018; Kuerban et al., 2020; M. Li et al., 2018; Song et al., 2016; Q. Wang et al., 2018; Y. Xie et al., 2019; Yue et al., 2020b):

$$D_{i,j} = \left[\left(RR_j - 1\right) / RR_j\right] \times I_{j,k} \times P_i \times P_{i,a} \tag{4}$$

$$RR_j = exp[\beta \times (C - C_0)] \tag{5}$$

where RR_j is the concentration-response functions and relative risk (RR) of a health outcome (mortality for disease j), based on the integrated exposure–responses across the full range of $PM_{2.5}$ or MDA8 O_3 concentrations(R. Burnett et al., 2018; R. T. Burnett et al., 2014). $I_{j,k}$ is the reported regional average annual disease mortality rate for disease j in region k (i.e., provincial baseline mortality). The $I_{j,k}$ values are different between age strata for ischaemic heart disease and stroke and are the same for the entire group for other kinds of disease(R. T. Burnett et al., 2014; Nawahda et al., 2012, p. Estimation of $PM_{2.5}$-associated disease burden in China in 2020 and 2030 using population and air quality scenarios: a modelling study); P_i is the population of city i; $P_{i,a}$ is the proportion of the population in city i with age a for the given year; the value of β represents the excess risk of mortality per increase in 1 μg m^{-3} of $PM_{2.5}$ or 10 μg m^{-3} MDA8 O_3; C and C_0 are the annually averaged concentrations and the references of $PM_{2.5}$ or MDA8 O_3, respectively. Here, annual mean concentrations of $PM_{2.5}$ and MDA8 O_3 for each prefecture were calculated using the monitoring concentration data (each prefecture has at least one monitoring site). Following references (Kuerban et al., 2020; Lefohn et al., 2018; Lu et al., 2018), the annual mean MDA8 O_3 (C in Equation (5)) was calculated using the data from April 1 to September 30. We applied the C_0 values of 10 μg m^{-3} for $PM_{2.5}$ and 100 μg m^{-3} for O_3 following the WHO Air Quality Guidelines(Organization, 2006).

2.9. Analysis methods

The site level monthly, seasonal and annual values were aggregated to county and region scales (fig. S1 and table S3) as the mean values of all the sites located in the certain county/region. Before analyzing monotonic linear trends from the five year time series data, we deseasonalized the data to void the bias from the seasonality following ref. (Silver et al., 2018). The Mann-Kendall test was used to assess the significance of trends (using a threshold p-value of 0.05), and the magnitude of the trend was calculated using the Theil–Sen estimator. Both tests are resistant to outliers, and do not require any assumptions about the data used. Absolute trends were converted to relative trends by dividing by the 2015 to 2019 mean. The t-test was used to assess the significance of difference in pollution and in their features between regions with a threshold $p = 0.05$.

In order to explore the change in the distribution of the annual means of $PM_{2.5}$ and MDA8 O_3, we use the Kernel density estimation method (Davis et al., 2011). The probability distribution function (PDF) is calculated as follows:

$$P(min \le x \le max) = \int_{min}^{max} f_X(x)dx \tag{6}$$

where $P(min \le x \le max)$ is the probability of occurrence for X with values between min and max, and $f_X(x)$ is frequency of occurrence of X at a specific value of x between min and max. The air pollutant X can be $PM_{2.5}$ and MDA8 O_3.

The emission-driven trends ($PM_{2.5}$ decreases while ozone increases) would produce a negative relationship between $PM_{2.5}$ and ozone. We therefore corrected for the effect of their 2015–2019 trends (K. Li et al., 2019; Y. Wang et al., 2020; Zhao et al., 2020) before doing a rigorous analysis of the observed relationships between the two and of atmospheric total oxidant ($O_x = O_3 + NO_2$) (Table 2 & Fig. S10). The 2015–2019 increase in ozone is also driven by other factors, including trends in NO_x emissions and meteorology(K. Li et al., 2019). We detrended the time series for $PM_{2.5}$, ozone and NO_2 by removing the ordinary linear regressions of daily concentrations versus time for each quality-assured measurement station over the 2015–2019 period and then adding back the 2015–2019 mean concentrations.

3. Results

3.1. Improved $PM_{2.5}$ and worsened O_3 air quality

The 24-h $PM_{2.5}$ and maximum daily 8-h moving average O_3 (MDA8 O_3) exhibit distinct spatial patterns and their 5-year averages for most of the 1405 sites exceed the air quality guidelines of the World Health Organization (WHO) and of the China's National Ambient Air Quality (NAAQS, Fig. 1A and B, fig.S2 andtable S1). High levels of $PM_{2.5}$ concentrations were observed in northern and central China, especially in the BTH and Fen Wei Plain (FWP) regions with annual mean values of

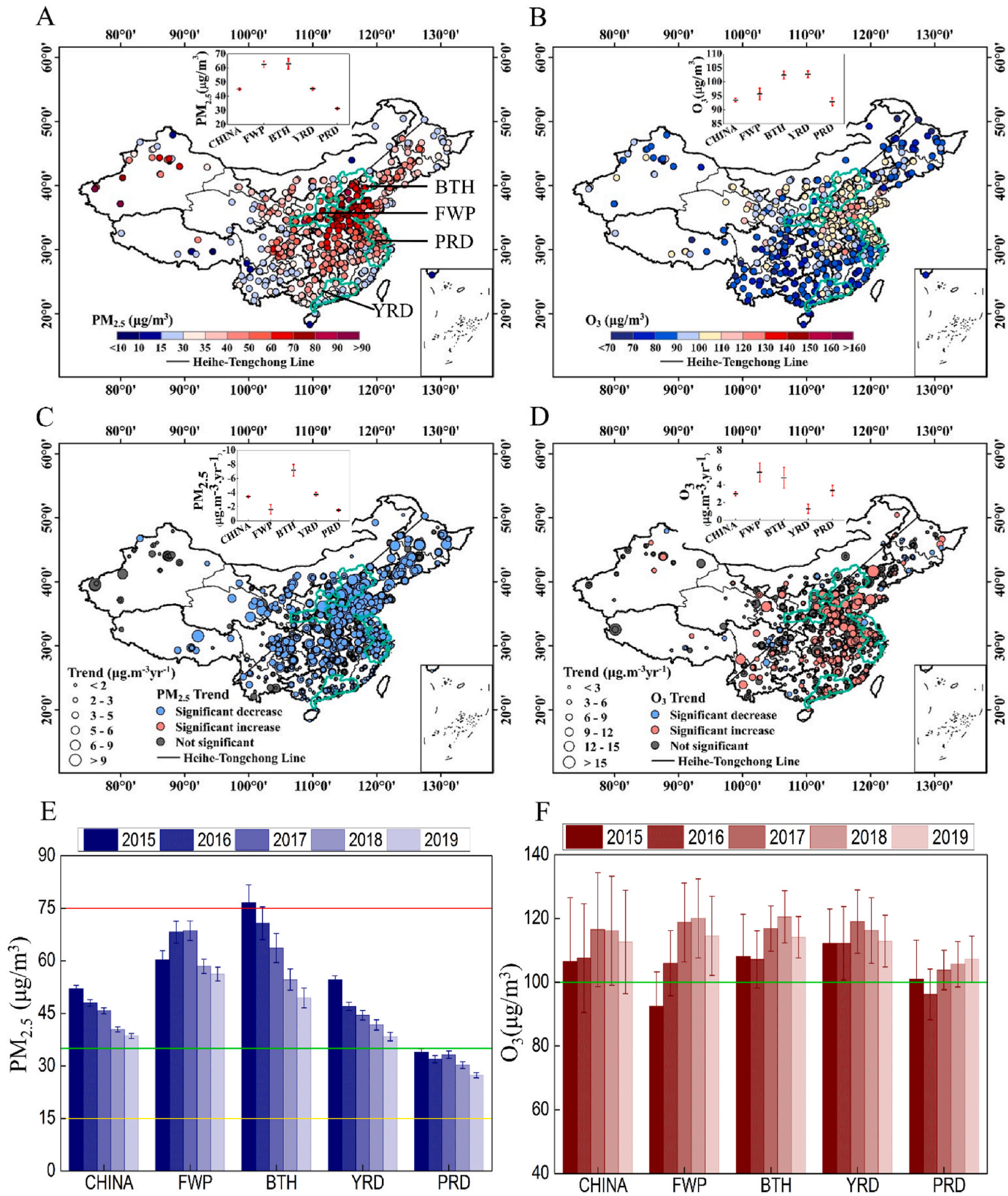

Fig. 1. Spatial patterns of 5-year concentration averages of $PM_{2.5}$ (A) and MDA8 O_3 (B) and their linear trends (C, D) at the 1405 sites from 2015 to 2019. E, F show the regional annual averages of $PM_{2.5}$ (E) and MDA8 O_3 (90% percentile, F) for China and the four key regions of Fen Wei Plain (FWP), Beijing-Tianjin-Hebei (BTH), Yangtze River Delta (YRD) and Pearl River Delta (PRD) (table S3, fig.S1). The inserts in A-D show the corresponding regional average values for China and the 4 key regions. Error bars indicate the regional cluster variation ranges (95% CI). The red, green and yellow horizontal lines on E and F show Chinese NAAQS (National Ambient Air Quality Standard) and WHO (World Health Organization) Air Quality Guidelines values (table S1). The statistical significance threshold is $p = 0.05$.

63 μg m^{-3} (Fig. 1A and E, Fig.S1,Fig.S2 A-F). BTH had the largest range in $PM_{2.5}$, from <20 to >100 μg m^{-3}, while PRD had lowest annual mean value of 32 μg m^{-3}, with a narrow range from 18 to 42 μg m^{-3} (Fig.S5A). High levels of MDA8 O_3 concentrations were observed in eastern and northern China, the BTH and YRD regions with annual means of about 102 μg m^{-3}(Fig. 1B; Fig.S2 G-L), and the 90-percentile of annual MDA8 O_3 concentration larger than 100 μg m^{-3} for China (119, 95% CI: 94–130 μg m^{-3}) and for all the four key regions (Fig. 1F). A strong seasonality of both $PM_{2.5}$ and MDA8 O_3 was observed and with dramatic regional variations (Figs.S4). The highest winter $PM_{2.5}$ values were observed in the FWP region, while the BTH region had highest values for other seasons (Fig.S4A,Fig.S5). The highest spring MDA8 O_3 concentration values were observed in the YRD and BTH regions, the highest summer MDA8 O_3 values were observed in the BTH and FWP regions, and the highest autumn and winter MDA8 O_3 values were observed in the PRD region (Fig.S4B, Fig.S6).

As shown in Fig. 1A–C,E, Fig. 2A and fig.S2 A-F, a substantial reduction in $PM_{2.5}$ concentrations from 2015 to 2019 occurred across

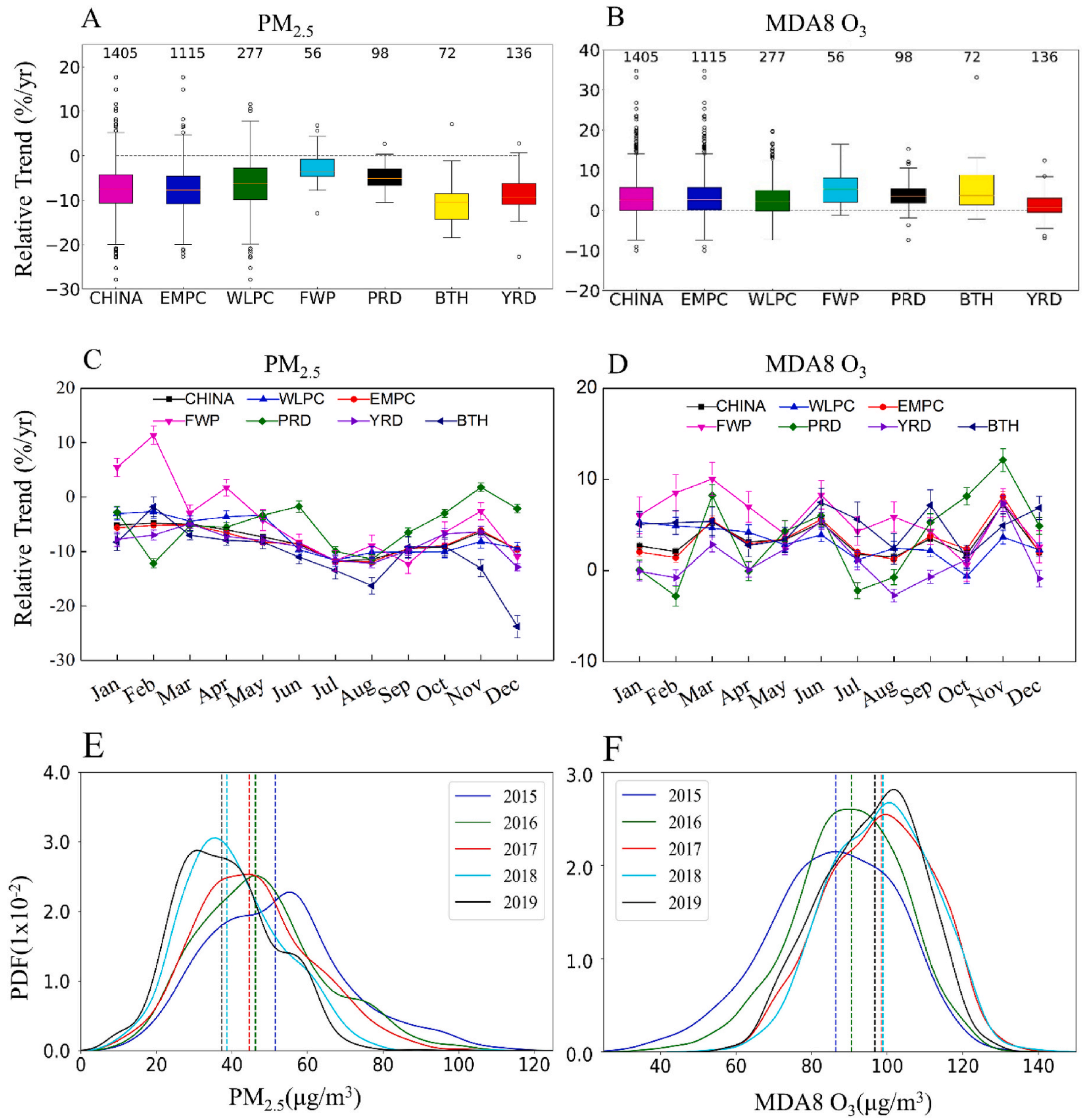

Fig. 2. Regional averaged linear trends in annual and monthly averages of $PM_{2.5}$(A, C) and MDA8 O_3 (B, D) from 2015 to 2019 for China and 6 key regions (table S3, fig.S1). The number quality-assured sites for each region is indicated at the top of the plot. E, F, the Kernel density estimates of the PDF (probability density function) of $PM_{2.5}$ (**E**) and MDA8 O_3 (**F**) over China during 2015–2019. The statistical significance threshold is $p = 0.05$.

99.7% of the total data-qualified sites (749 significantly decreasing sites over the total 1405 sites; the national mean $PM_{2.5}$ concentrations decreased from 52.0 μg m^{-3} (95% CI: 50.1–53.0) in 2015 to 38.6 μg m^{-3} (95% CI: 37.8–39.3) in 2019 with a median national annual rate of −3.4 μg m^{-3} yr^{-1} (95% CI: 3.3 to −3.6 μg m^{-3} yr^{-1}, equal to −4.1.0% to −7.8% yr-1, of the 5-year mean); the largest reduction occurred in the BTH region with a mean annual rate of −7.2 μg m^{-3} yr^{-1} (95% CI: 6.3 to −8.0 μg m^{-3} yr^{-1}, equal to −10.1% - - 12.7% yr^{-1}, of the 5-year mean); while the smallest reduction was found in the FWP region with a mean annual rate of −1.6 μg m^{-3} yr^{-1} (95% CI: 1.0 to −2.3 μg m^{-3} yr^{-1}, equal to −1.5% - - 3.7% yr^{-1}, of the 5-year mean).

In contrast, about 84% of sites show increasing trends (16% significant increasing sites, $P < 0.05$) in annual mean MDA8 O_3 concentrations (Fig. 1B–D, F, Fig. 2B and Fig. 2G–L), with a median national increasing trend of 3.0 μg m^{-3} yr^{-1} (95% CI: 2.8–3.2 μg m^{-3} yr^{-1}, equally to 3.0%–3.5% yr^{-1} of the 5-year average, Fig. 2B). The FWP and BTH regions show higher increasing rates of 5.5 μg m^{-3} yr^{-1} (95% CI: 4.4–6.5 μg m^{-3} yr^{-1}, equal to 4.6%–6.8% yr^{-1}, of the 5-year average), and of 4.8 μg m^{-3} yr^{-1} (95% CI: 3.6–6.0 μg m^{-3} yr^{-1}, equal to 3.6%–5.9% yr^{-1}, of the 5-year average); and their the 90-percentile of annual MDA8 O_3 concentrations from 92 to 108 μg m^{-3} increased to 120 and 121 μg m^{-3}, respectively (Fig. 1F). While the smallest reduction was found in the YRD region with a mean annual rate of 1.3 μg m^{-3} yr^{-1} (95% CI: 0.8–1.8 μg m^{-3} yr^{-1}, equal to 3.0%–4.3% yr^{-1}, of the 5-year average).

The peak of the estimated Kernel density (PDF: probability distribution function) for annual mean $PM_{2.5}$ concentrations over China became steeper and moved to left, indicating that $PM_{2.5}$ concentrations of most cities decreased (Fig. 2E). Notably, the upper tail of the distributions decreased over time, implying that the sites with high $PM_{2.5}$ values ranging from 75 to 120 μg m^{-3} had a great reduction (Fig. 2E). In contrast to $PM_{2.5}$, Fig. 2F shows that the peaks move to the right, indicating an increase in the annual mean MDA8 O_3 concentration in China. Compared to 2015, the MDA8 O_3 values increased by 4.8%, 13.9%, 14.4% and 12.0% per year in the following four years.

The patterns of the estimated Kernel density curves for annual and seasonal $PM_{2.5}$ and MDA8 O_3 concentrations were significantly different among different regions (*t*-test $P < 0.05$, figs.S5-S7). In some cases, the PDFs for $PM_{2.5}$ and MDA8 O_3 are bimodal. While it is difficult to draw strong conclusions, this may indicate heterogeneity in their change regime within some regions. The patterns for O_3 are less consistent than for $PM_{2.5}$ (fig.S7) showing a general pattern of decreasing annual means from 2015 to 2019; however, in all cases the peaks of PDF curves (i.e., annual means) for 2015 and 2016 lay to the left of 2017, 2018 and 2019. This indicates that the annual averageMDA8 O_3 concentration has tended to increase over time. There were significant differences (*t*-test $P <$ 0.05) in monthly decreasing trends of $PM_{2.5}$ (Fig. 2C) and monthly and seasonal increasing trends of MDA8 O_3 (Fig. 2D) among the six key regions.

3.2. The regional patterns of changes in deaths attributable to $PM_{2.5}$ and O_3 pollution

The 5-year averages of $PM_{2.5}$ and O_3 -related deaths in China by specific causes (see Materials and Methods) were 1.24 (95% CI: 1.20–1.28) million and 0.18 (95% CI:0.174–0.185) million, respectively (Fig. 3G and H), which are close to the estimates from the GBD (Stanaway et al., 2018) and other studies (J. Huang et al., 2018; Organization, 2006). The 5-year mean premature deaths per 100 km^2 associated with $PM_{2.5}$ and O_3 for the whole China were 39 persons (95% CI: 34–44) and 6 persons (59% CI: 5–7), respectively. The spatial pattern of 'per-unit-area mortality' attributed to $PM_{2.5}$ and O_3 exposures (Fig. 3A and B), were similar to that for total deaths (fig. S8A, B), shows a very strong heterogeneity and it correlates with both the high levels of pollution and population. The large number of deaths were observed in the area to the southeast of the Heihe -Tenchong Line, which covers the most polluted and fastest-developing regions. High levels of premature deaths attributed to $PM_{2.5}$ and O_3 pollution exposure were observed in eastern, northern and central China, especially in the BTH and PRD regions, with annual mean values of 84 (95% CI: 55–113) and 80 (95% CI: 55–105) deaths/100 km^2 for PM2.5 and 18 (95% CI: 11–24) and 17 (95% CI: 11–24) deaths/100 km^2, respectively (Fig. 3A and B). In comparison, the western, northwestern and southern parts of China had lower disease burdens (Fig. 3A and B; fig.S9 A, B) owing to lower $PM_{2.5}$ concentration (Fig. 1A), lower O_3 concentration (Fig. 1B) and lower population densities. The high ratio values of $PM_{2.5}$ -related versus O_3 -related deaths were observed in the area to the northwest of the Heihe -Tenchong Line (Fig. 3C).

As shown in Fig. 4 A&C and fig.S8A&B, at the provincial level, the top three provinces with the highest $PM_{2.5}$-related deaths (>100,000) and O_3 -related deaths (>20,000) were Henan, Shandong and Hebei, and these regions also had a high level of air pollution and population density. The rural provinces, where the population was low and the air pollution concentration was low (annual $PM_{2.5}$ concentration <15 μg m^{-3} and annual MDA8 O_3 concentration <50 μg m^{-3}; Fig. 1A, fig.S2 G-L), such as Ningxia, Qinhai, Hainan and Tibet had very low premature mortality associated with $PM_{2.5}$ and O_3. The three metropolises of Shanghai, Tianjin and Beijing had highest per-unit-area mortality for $PM_{2.5}$ and to O_3. Qinghai, Inner Mongolia and Tibet were the three lowest provinces for $PM_{2.5}$ related deaths and Guangxi, Guizhou and Hainan were the three lowest provinces for O_3 related deaths. The top three provinces with the highest per-capita mortality attributed to $PM_{2.5}$ are Hebei, Henan and Shandong and to O_3 were Beijing, Shandong and Hebei.

Table 1 and Fig. 3 show contrasting trends in the numbers of all-cause premature mortality attributable to $PM_{2.5}$ and O_3 exposures during 2015–2019: the former decreased from 1.45 million (45.1 deaths/100 km^2 (95% CI: 39.2–51.0)) in 2015 to 1.04 million (33.6 deaths/100 km^2 (95% CI: 29.3–37.9)) in 2019, while the latter increased from 0.13 million (7.6 deaths/100 km^2 (95% CI: 6.1–9.0)) in 2015 to 0.21 million in 2019 (9.0 deaths/100 km^2 (95% CI: 7.7–10.3); Table 1, Fig. 3G and H). The numbers of annual deaths per unit-area attributable to both $PM_{2.5}$ and O_3 exposures across China and the three key regions (i.e., BTH, YRD and PRD) decreased though the deaths attributed to O_3 exposure increased from 2015 to 2019, and the changing patterns were highly heterogeneous, especially in the area to the southeast of the Heihe-Tenchong Line (Fig. 3D).

The kernel density estimated PDF curves for $PM_{2.5}$-related deaths over China became steeper and moved to the left while O_3 -related deaths became flatter and moved to the right, indicating the $PM_{2.5}$-related deaths decreased (Fig. 3I) while O_3 -related deaths increased (Fig. 3J). As shown in Fig. 3D–F, the spatial patterns of the trends in the per-unit-area mortality premature deaths (Fig. 3C and D) and the total deaths at a city level (fig.S8 C, D) attributed to $PM_{2.5}$-related and O_3 -related deaths from 2015 to 2019, exhibit very strong heterogeneities with the largest deceasing trends of deaths in BTH and YRD. These spatially heterogeneous patterns were controlled by the spatio-temporal changes in 24-h $PM_{2.5}$ concentration (Fig. 1C and fig. S2F) and MDA8 O_3 concentration (fig. 1D and fig. S2L) during 2015–2019 and were also associated with population density. The $PM_{2.5}$-related deaths decreased from 2015 to 2019 for all provinces, with a mean rate of −11% (95% CI: 7–14%) ranging from −4% to −31% (Fig. 4B), whereas O_3 -related deaths for major provinces showed an increasing trend with rates higher than 10% (Fig. 4D).

3.3. Changes in anthropogenic emissions of precursor gases of O_3 and secondary PM

The formation of surface ozone and secondary PM is related to anthropogenic emissions of VOCs, carbon monoxide (CO), sulfur dioxide (SO_2), ammonia (NH_3) and nitrogen oxide ($NO_x \equiv NO + NO_2$) (K. Li et al., 2019; K. Li et al., 2019; Tan et al., 2018; Y. Wang et al., 2020). In the troposphere, ozone is produced from the reaction of CO, NO_x, VOCs and CH_4, with other chemical compounds in the presence of solar radiation (the intensity of UV radiation)(K. Li et al., 2019; Seinfeld et al., 1998; Seinfeld and Pandis, 2016; Tan et al., 2018). Chinese anthropogenic emissions estimated in the Multi-resolution Emission Inventory for China (MEIC) inventory (see Materials and Methods) decreased by 24.4% for CO, by 24.2% for NO_x and increased by 1.6% for VOCs over the 2012–2017 period (Fig. 5G–L, & fig.S9 J-R). From 2012 to 2017, the emissions of primary $PM_{2.5}$ decreased by 35.8% and its precursors were observed to have decreased by 63.1% for SO_2 and by 4.1% for NH_3 (Fig. 5A–F & Fig.S 9 D-I). As shown in Fig. 5 and Fig.S9, the spatial distributions of emissions and their changing trends exhibit highly heterogeneous and the most reduction regions were found in BTH and YRD ($PM_{2.5}$ >40%, SO_2>67%, NO_x>25%); however, NH_3 and VOCs, as both precursors of PM and O_3, changed very slightly with regional averaged rates of −3.3% and 3.9% for BTH and −12.5% and 6.9% for YRD, respectively.

The MEIC inventory data for the trends and spatial distribution of anthropogenic emissions of $PM_{2.5}$, CO, SO_2 and NO_x during 2015–2019 were consistent with those of *in situ* measured (Fig. 1A, B, and Fig. S3) and remotely sensed concentrations (Dehkhoda et al., 2020; Hilboll et al., 2013; Krotkov et al., 2008; C. Li et al., 2017).

4. Discussion, conclusion, and policy implications

4.1. Observed regionally varied $PM_{2.5}$-O_3 and $PM_{2.5}$-O_x relationships

The tropospheric ozone and the secondary PM pollutants have different formation mechanisms, and their interactions lead to close connections and relations. The total oxidant (O_x) ($O_x = O_3 + NO_2$) can be regarded as a quantitative expression of the atmospheric oxidation capacity, which control secondary particle formation (Ding et al., 2013; X. Huang et al., 2020; K. Li et al., 2019; K. Li et al., 2019; Y. Wang et al., 2020; Zhu et al., 2019). We averaged the daily $PM_{2.5}$, MDA8 ozone and

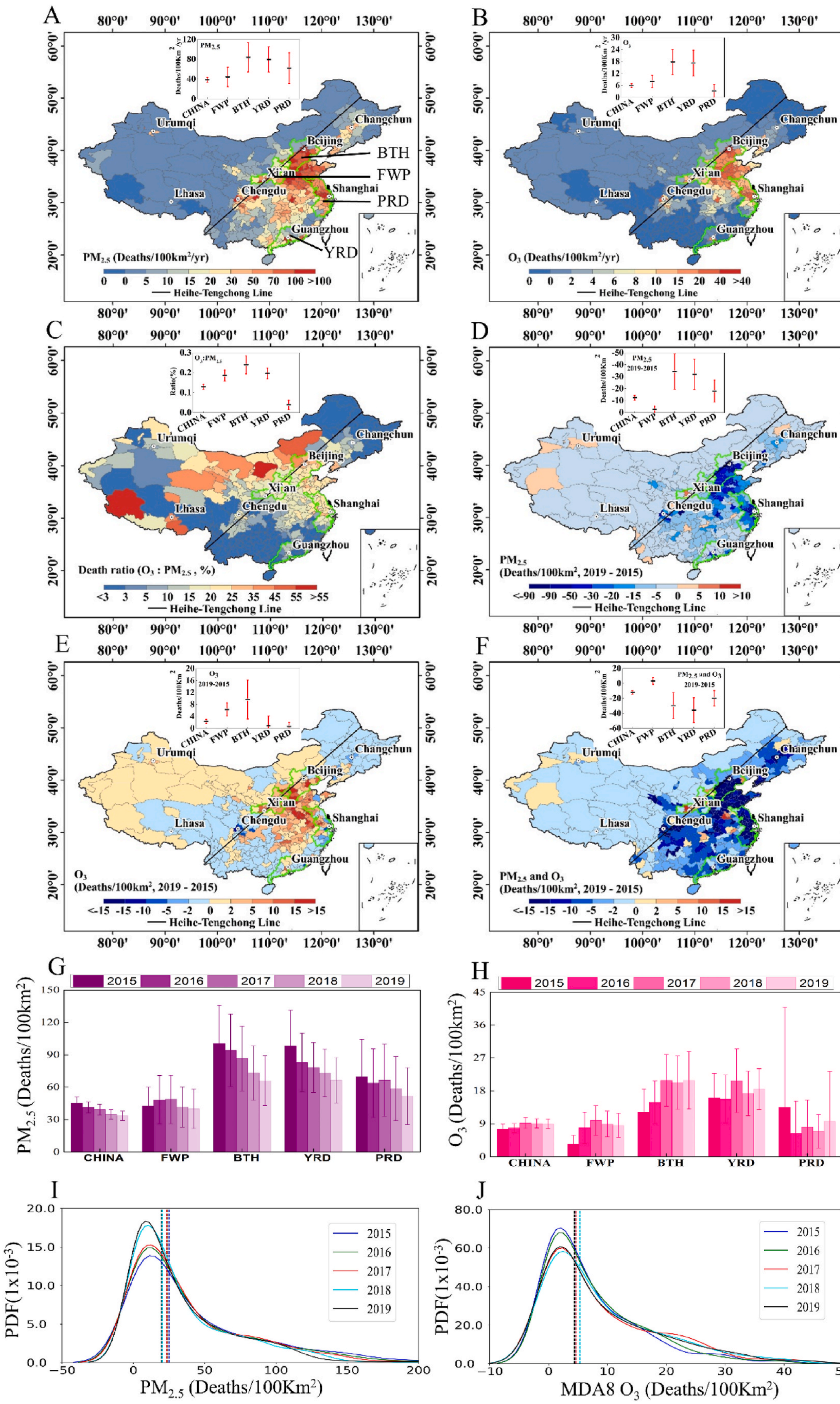

(caption on next page)

Fig. 3. Spatial patterns of 5-year averages of premature mortalities per unit-area and their linear trends attributed to long-term exposures of $PM_{2.5}$ and O_3 at city levels from 2015 to 2019. A, B, the 5-year averages of all-cause deaths attributed to long-term exposures of $PM_{2.5}$ (A) and O_3 (B) per unit-area for 367 cities in death/100 km^2/yr. C, the 5-year averages of relative contributions of O_3-artibuted mortalities to $PM_{2.5}$-artibuted mortalities (in %). D-F, the difference between 2019 and 2015 in annual all-cause mortalities per unit-area attributed to exposures of $PM_{2.5}$ (D), O_3 (E) and both of O_3 and $PM_{2.5}$ (F). G-H, the regional annual total numbers of all-cause deaths attributed to long-term exposures of $PM_{2.5}$ (G) and O_3 (H) for China and the 4 key regions (table S3, fig.S1), where error bars indicate the annual variation ranges (95% CI). In A-E, the insert shows the corresponding regional average values for China and the 4 key regions, where error bars indicate the regional cluster variation ranges (95% CI). I, J, the Kernel density estimates of the PDF of all-cause deaths attributed to exposures of $PM_{2.5}$ (G) and O_3 (H) over China during 2015–2019. The statistical significance threshold is $p = 0.05$.

NO_2 data over all sites to obtain the daily time series with removal of the 2015–2019 trends (see Materials and Methods) to avoid the influence from the $PM_{2.5}$ concentration decrease over the period.

Fig.S10 and Table 2 show the spatial-temporal distributions of correlations of daily $PM_{2.5}$ with MDA8 O_3 and O_x. The $PM_{2.5}$ concentrations were significantly positively correlated with O_3 and O_x concentrations (95% CI) for most regions and seasons over China during 2015–2019, especially for summer time(K. Li et al., 2019; Schnell and Prather, 2017; Zhu et al., 2019), while significant negative $PM_{2.5}$-O_3 correlations (95% CI) were mainly observed in northern China during winter (DJF), autumn (SON) and during heavy pollution episodes, when 24-h daily mean $PM_{2.5}$ concentration >50 μg m^{-3} or MDA8 ozone >100 μg m^{-3}. The positive correlation between $PM_{2.5}$ and O_x was generally much stronger than $PM_{2.5}$-O_3 correlation (Table 2, Fig. S10). The strongest positive $PM_{2.5}$-O_3 and $PM_{2.5}$-O_x correlations ($r > +0.7$) were observed in southern China during summer (JJA), and the strongest negative correlations ($r < -0.5$) were observed in northern China during winter (DJF). Interestingly, the spatial-temporal distribution patterns of $PM_{2.5}$-O_3 correlations strongly resembled those of temperature (Fig. S11). Most sites with positive $PM_{2.5}$-O_3 correlations were observed over warm southern China (e.g., PRD region) reaching the strongest correlations in summer and most sites with negative $PM_{2.5}$-O_3 correlations were found over cold northern China, where the strongest correlations were found in winter (e.g., BTH and FWP regions).

$PM_{2.5}$ and ozone exhibited varying and even inverse correlations among different regions, seasons, pollution episodes and different warm air temperature conditions(Schnell and Prather, 2017; Zhu et al., 2019). The positive $PM_{2.5}$-O_x correlations exhibited, under almost all conditions except for heavy episodes. The $PM_{2.5}$ and ozone positive correlations prevailed for high air temperature samples, while the negative correlations were generally found in cold environments and heavy polluted days. These phenomena indicate their different interaction mechanisms of secondary pollution formation over time and across space, which are discussed below.

Inhibition of $PM_{2.5}$ on ozone generation by reducing photolysis rates mostly occurred in cold environments. Particulate's scatter or absorb solar radiation directly and consequently decrease the actinic flux of ultraviolet (UV) radiation and inhibit the photolysis reactions near the surface by reducing the photolysis rates. The ozone generation is finally suppressed (J. Li et al., 2011; M T. Li et al., 2018; Menon et al., 2008; Real and Sartelet, 2011; Tie et al., 2005; Zhu et al., 2019). For north China in winter, heating in cold weather (Fig. S12D) and low boundary layer height associated with low temperature led to high $PM_{2.5}$ concentration. This suppressed O_3 generation. It was reported that surface photolysis rates $J(NO_2)$ and $J(O_3)$ in Eastern China were reduced by10–30% and 20–30% respectively, due to the effect of particulates on photolytic radiation in winter (Tie et al., 2005).

Suppressing ozone generation by NO titration effect in the cold season at low temperatures. It was reported (Zhu et al., 2019) that the NO concentration was about 11 μg m^{-3} for BTH in January, which is five time higher than that for PRD in July. It is known that O_3 production is removed by freshly emitted NO through the "$O_3 + NO \rightarrow NO_2 + O_2$" reaction(T. Wang et al., 2017; M. Xie et al., 2016). NO and BC, as well as $PM_{2.5}$, have similar sources, such as combustion and traffic activities(H. Chen et al., 2019; Ding et al., 2013). Northern China in winter has low air temperatures and was characterized by weaker atmospheric oxidation ability and consequently more NO was freshly emitted. Therefore, less NO was converted to NO_2, which contrasts with southern regions of China in summer, such as PRD, where more NO was converted to NO_2. The self-suppression of ozone production as the NO/NO_2 ratio shifts towards NO_2 was also reported to increase ozone under highly polluted conditions(K. Li et al., 2019). The negative $PM_{2.5}$-O_3 correlation for northern China in winter (Fig. S E) may be partly attributed the strong NO titration effect on removal of ozone.

Uptake of HO_2 by $PM_{2.5}$ suppressing ozone formation. HO_2 uptake by particles provides a sink for HO_x radicals and hence suppresses ozone formation(Abbatt et al., 2012; Jacob, 2000; K. Li et al., 2019; K. Li et al., 2019; Taketani et al., 2012). It is unclear whether the product of HO_2 uptake is H_2O_2 or H_2O (Mao et al., 2013). In GEOS-Chem simulations this effect on ozone formulation is small (K. Li et al., 2019). A complex aqueous-phase conversion of NO_2, nitrate radicals (NO_3) and dinitrogen pentoxide (N_2O_5) to nitric acid (HNO_3) leads to the uptake of NO_x by $PM_{2.5}$ (Jacob, 2000). The effect of NO_x uptake on ozone is large and occurs in the cold season and under heavy pollution conditions. This is partly due to the substantial decrease (24%) in NO_x emissions during 2015–2019 (Fig. 5G). This has made ozone production more NO_x sensitive. This is also evident from GEOS-Chem simulation(K. Li et al., 2019).

High total oxidant (O_x) and active photochemical activity promoting secondary pollution in hot environments. The secondary organic aerosol (SOA) is reported to have a strong correlation with O_x which indicates SOA formation is mainly promoted by photochemical oxidation. High concentration of O_3 generally accompanies in a high temperature environment with a strong atmospheric photochemical reactivity, and significantly promotes the level of atmospheric oxidation, which in turn enhances the formation of both secondary inorganic particulates and secondary organic particulates (D. Wang et al., 2016). This effect of ozone on the secondary particulates formation eventually leads to significant positive $PM_{2.5}$-O_3 correlations. These were observed in hot environments (Fig.S11), i.e., in summer for almost whole China (Fig.S10 C) and in other seasons only for southern China (Fig.S10 A, D-E).

4.2. Towards a region oriented simultaneously joint $PM_{2.5}$ and ozone pollutants control strategy

Previous research reported contrasting trends of $PM_{2.5}$ and surface-ozone concentrations in China (Y. Wang et al., 2020). This paper quantifies regionally variable trends and associated mortality of severe wintertime $PM_{2.5}$ and summertime surface-ozone during 2015–2019. A substantial $PM_{2.5}$ decrease during the 5-year period by annual rate of 3.3 μg m^{-3} (about 7.6% of the 5-year average) mainly attributed to specific-purpose clean air policies imposed since 2013 (Q. Zhang et al., 2019). Unfortunately, surface-ozone concentration increased rapidly owing to complicated formation mechanisms involving many factors. These include increased UV radiation (Y. Wang et al., 2020), changes in anthropogenic precursors (NO_x and VOCs) emissions (K. Li et al., 2019), the effect of decreasing $PM_{2.5}$ (K. Li et al., 2019), and regional specific NO_x/VOCs ratio, which controls the NO_x-limited or VOCs-limited regimes (Y. Wang et al., 2020).

The $PM_{2.5}$ control have had unintended effects on the surface ozone, an irritant of the respiratory system. The total number of deaths attributable to both $PM_{2.5}$ and O_3 exposure across China showed a slight decreasing trend while the deaths associated to O_3 exposure increased

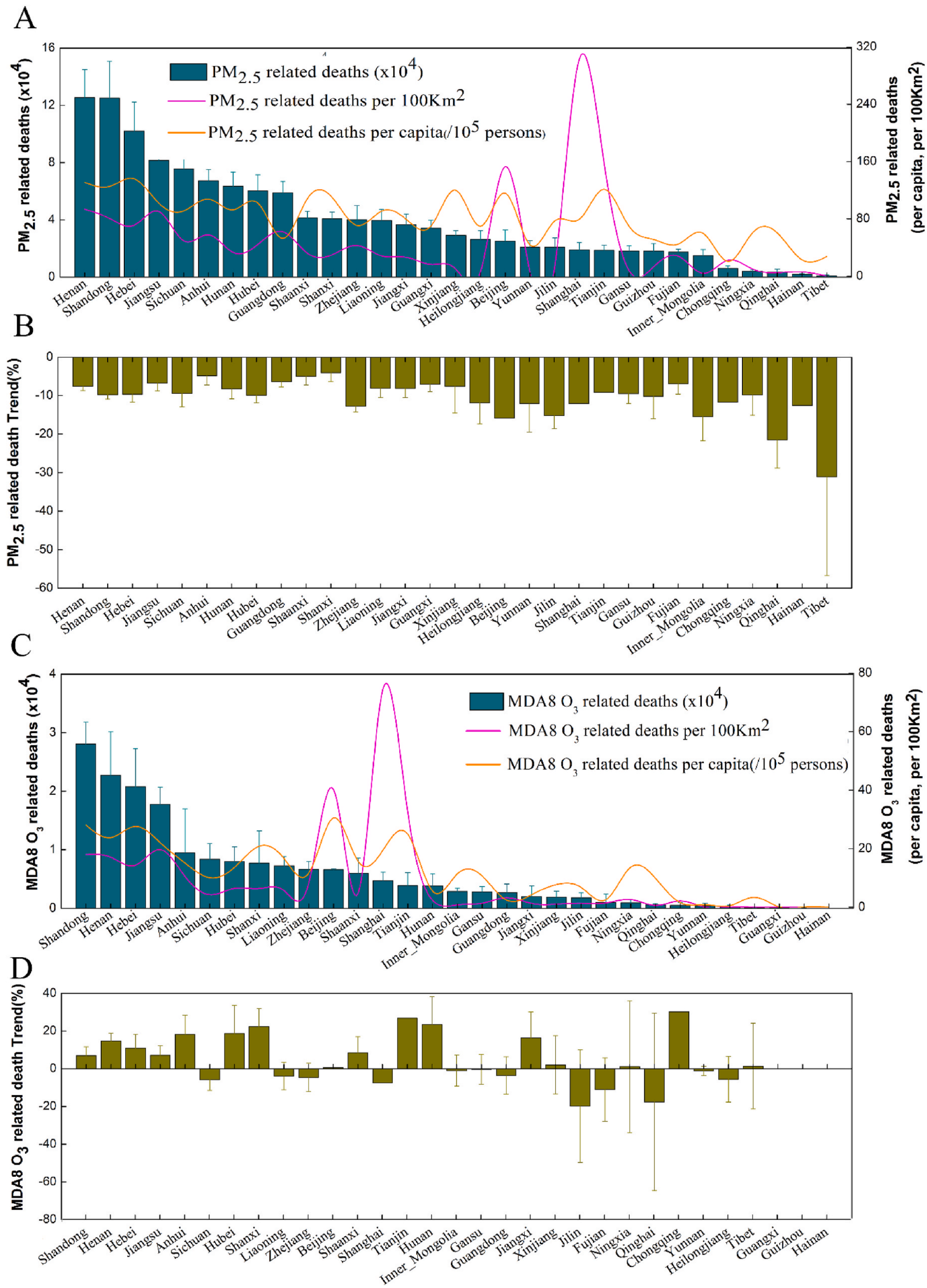

Fig. 4. 5-year (2015–2019) averaged annual premature mortality attributed to exposures of $PM_{2.5}$ (A) and ozone (C) for each province in China and the linear trends attributed to $PM_{2.5}$ (B) and to ozone (D) from 2015 to 2019. In A and C, the main vertical axes indicate the 5-year mean annual number of premature deaths attributed to $PM_{2.5}$ or ozone and the secondary vertical axes indicate the respective per-capita deaths and per-unit-area mortality. The statistical significance threshold is $p = 0.05$.

Table 1
Comparison of the annual total number of deaths attributable to $PM_{2.5}$ and O_3 in China and the 6 key regions (see table S3 and fig.S1), Unit: million deaths.

	Region	2015	2016	2017	2018	2019	Mean
$PM_{2.5}$	China	145.3201	133.704	126.9184	110.2835	103.6923	123.9837
	FWP	22.972	22.2567	21.1627	19.2654	18.1391	20.7592
	BTH	17.4152	16.4545	15.045	12.7284	11.3676	14.6021
	YRD	17.3044	14.6431	13.9515	12.8923	11.7737	14.11
	PRD	6.5321	6.0599	6.3208	5.6343	4.9028	5.8900
MDA8 O_3	China	12.5277	15.335	21.4119	20.5708	20.0995	17.9890
	FWP	1.8257	3.111	4.5958	4.3109	4.3944	3.6476
	BTH	2.1163	2.6404	3.6524	3.5911	3.6232	3.1247
	YRD	2.7463	2.506	3.5424	2.8936	2.8474	2.9071
	PRD	0.1782	0.1425	0.3813	0.4004	0.2567	0.2718

Table 2
Statistical correlations for 24-h $PM_{2.5}$ versus MAD8 O_3 and 24-h $PM_{2.5}$ versus daily O_x concentrations at all sites during 2015–2019 in China and the four key cluster regions[a].

Region	Time	All time		Pollution data		Spring		Summer		Autumn		Winter	
	Correlation	$PM_{2.5}$ vs O_3	$PM_{2.5}$ vs O_x	$PM_{2.5}$ vs O_3	$PM_{2.5}$ vs O_x	$PM_{2.5}$ vs O_3	$PM_{2.5}$ vs O_x	$PM_{2.5}$ vs O_3	$PM_{2.5}$ vs O_x	$PM_{2.5}$ vs O_3	$PM_{2.5}$ vs O_x	$PM_{2.5}$ vs O_3	$PM_{2.5}$ vs O_x
China	Positive	25.66	53.93	2.64	9.35	53.93	82.10	88.67	91.87	47.17	80.67	30.31	89.28
	Negative	65.27	11.95	93.64	81.44	11.95	4.10	2.60	1.57	23.69	2.73	45.32	1.43
	Not-Sig	9.07	34.13	3.72	9.21	34.13	13.80	8.74	6.56	29.15	16.60	24.37	9.29
FWP	Positive	0	3.39	0	0	3.39	33.90	79.66	81.36	0	30.51	0	89.83
	Negative	100	64.41	100	100	64.41	5.09	1.70	0	91.53	0	96.61	1.70
	Not-Sig	0	32.20	0	0	32.20	61.02	18.64	18.64	8.48	69.49	3.39	8.48
BTH	Positive	6.58	50.00	0	1.32	50.00	94.78	82.90	88.16	6.58	86.84	0	94.74
	Negative	88.16	3.95	100	93.42	3.95	0	2.63	0	36.84	0	98.68	0
	Not-Sig	5.26	46.05	0	5.26	46.05	5.26	14.47	11.84	56.58	13.16	1.32	5.26
YRD	Positive	14.94	71.90	0	4.55	71.90	98.04	100	100	66.01	98.04	20.26	100
	Negative	61.69	1.31	100	79.87	1.31	0	0	0	1.31	0	10.46	0
	Not-Sig	23.38	26.80	0	15.58	26.80	1.96	0	0	32.68	1.96	69.28	0
PRD	Positive	100	99.00	17	78	99.00	100	100	100	100	100	100	100
	Negative	0	0	60	7	0	0	0	0	0	0	0	0
	Not-Sig	0	1	23	15	1	0	0	0	0	0	0	0

[a] The number of quality-assured sites for China and the four key cluster regions (table S3 and fig.S1) is 1405 (China), 56 (FWP), 72 (BTH), 136 (YRD) and 98 (PRD). The table shows the percentage of sites with significant positive, negative or not significant (Not-Sig) correlations over China and the 4 cluster regions ($p = 0.05$). Daily O_x = MDA8 O_3 +24-h NO_2 is the total atmospheric oxidant. The convective time series data for the whole year (annual), spring (MAM), summer (JJA), autumn (SON) and winter (DJF) were used for correlation analysis. The "pollution data" refer to the data when 24-h daily mean $PM_{2.5}$ concentration >50 μg m^{-3} or MDA8 ozone >100 μg m^{-3}.

from 2015 to 2019. The changes in mortality, $PM_{2.5}$ and ozone showed obvious spatially heterogeneous patterns across the four key regions, 31 provinces and 367 cities. Urban regions and rural areas had different ozone production regimes: NO_x -limited, VOC-limited or transition between them. In addition, the responses of $P(O_3)$ to changes in NO_x and/or VOCs, the various reactions of HO_2, OH, and RO_2, the responses of ozone production to multiple chemical and meteorological conditions, are region dependent and have high heterogeneities. Considering a non-linear tipping point of NO_x chemistry involved, to reduce both haze and ozone pollution requires the balance of emitted species with different ratios of VOCs and NO_x among different regions (X. Huang et al., 2020).

The results presented in this paper have important implications for developing a region oriented simultaneously joint two-pollutant control air pollution strategies to decrease both $PM_{2.5}$ and ozone coordinately in China. Sophisticated regulations of emission reduction controlling VOC and NO_x emissions based on local atmospheric chemistry would substantially improve both $PM_{2.5}$ and ozone air quality, otherwise, reducing its precursors may even cause an increase in summer surface ozone(K. Li et al., 2019; Lu et al., 2019; Organization, 2006), because atmospheric compound pollution has the characteristics of multiple pollution types superimposed, multiple process couplings and multi-scale pollution interactions, whose core driving force is atmospheric oxidation, and the representative pollutant is O_3.

Trade-offs may occur in the coordinated prevention of ozone and $PM_{2.5}$, hence a deep understanding of the chemical reaction between pollutants and the mechanisms of atmospheric oxidation would allow us to propose an optimized control strategy to simultaneously reduce both pollutants. It is required to establish a region-oriented VOCs and NO_x coordinated control strategy: on the basis of substantially reducing VOCs, gradually establish a long-term strategy for coordinated control of multiple pollutants with NO_x reduction. Our highly resolved results can provide detailed insights for supporting decision making and public health management in China. Our findings also have implications for other countries that face heavy air pollution, such as India, Pakistan, Bangladesh, and Indonesia. This around-the-world transfer of effective measures for cleaner air could benefit a vast amount of people.

Funding

This research is founded by the Special Fund for Carbon Peak and Carbon Neutrality Technological Innovation of Jiangsu Province (No. BE2023855, No. BE2022612), the Innovation Project of LREIS (No. KPI005), National Key R&D Program of China (2022YFB3903705), and the National Natural Science Foundation of China (No.41771114 and 41977404).

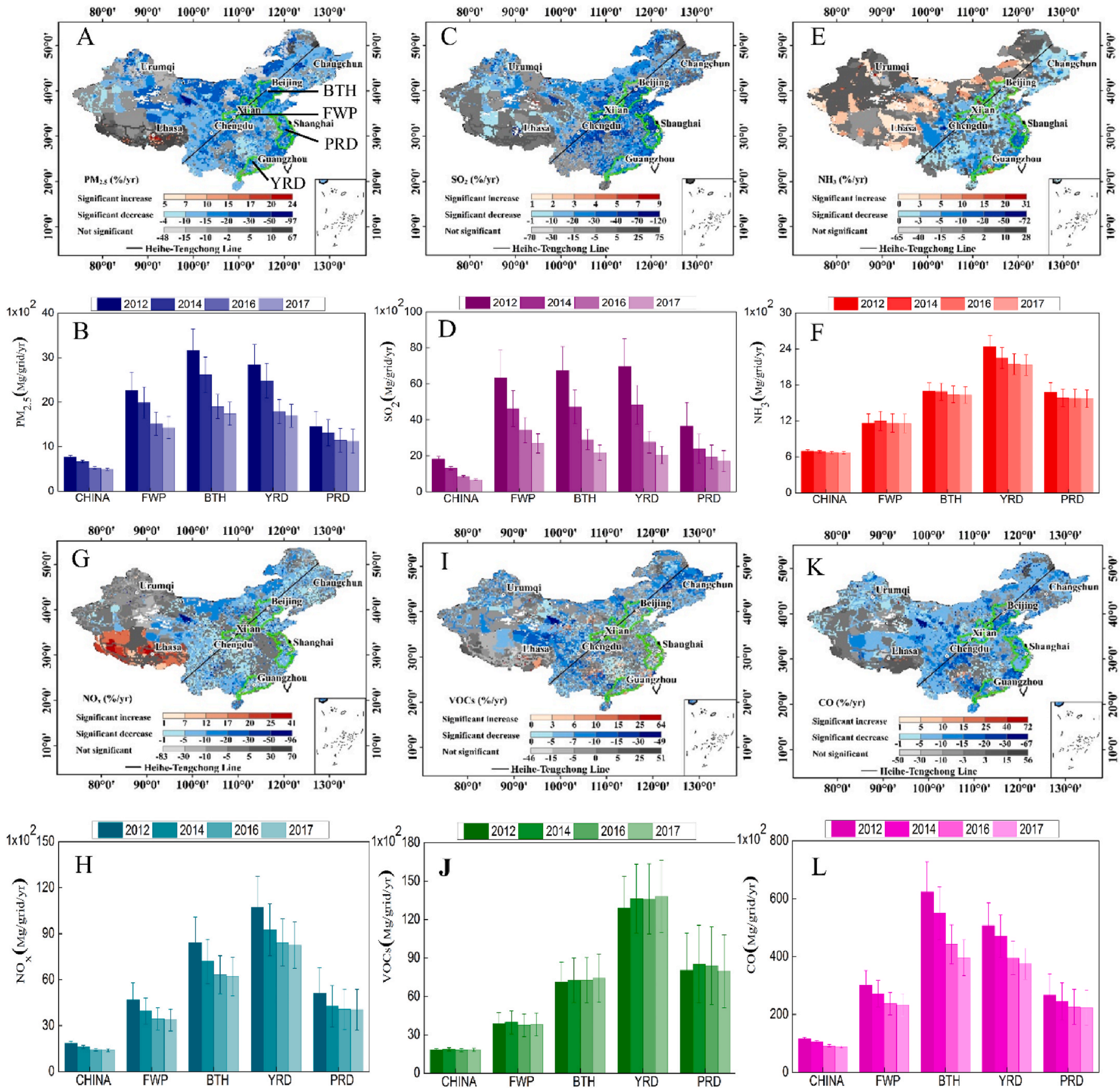

Fig. 5. Spatial distributions of linear trends of annual anthropogenic emissions at a 0.25° × 0.25° grid level and annual emissions of China and 4 key cluster regions from 2012 to 2017. A, C, E, G, H, I, the spatial distributions of linear trends in pollutant emissions of $PM_{2.5}$ (A), SO_2 (C), NH_3 (E), NO_x (G), VOCs (I); and CO (K). B, D, F, H, J, L, the regional annual means of $PM_{2.5}$ (B), SO_2 (D), NH_3 (F), NO_x (H), VOCs (J) and CO (L) during 2012–2017 for China and the 4 key regions (Table S3, Fig. S1). The anthropogenic emissions are estimated using MEIC (see Materials and Methods). The statistical significance threshold is $p = 0.05$.

Data and materials availability

All data needed to evaluate the conclusions in the paper are present in the paper and/or the Supplementary Materials. Additional data related to this paper may be requested from the corresponding authors.

CRediT authorship contribution statement

Baozhang Chen: Conceptualization, Formal analysis, Funding acquisition, Investigation, Methodology, Project administration, Resources, Supervision, Validation, Visualization, Writing – original draft, Writing – review & editing. **Sheng Zhong:** Data curation, Formal analysis, Investigation, Validation, Visualization, Writing – original draft. **Nicholas A.S. Hamm:** Data curation, Validation, Visualization, Writing – review & editing. **Hong Liao:** Data curation, Formal analysis, Validation, Writing – review & editing. **Tong Zhu:** Data curation, Formal analysis, Validation, Writing – review & editing. **Shu'an Liu:** Data curation, Validation, Visualization. **Huifang Zhang:** Data curation, Investigation, Visualization. **Lifeng Guo:** Data curation, Visualization. **Kun Hou:** Data curation, Validation, Visualization.

Declaration of competing interest

The authors declare that they have no known competing financial interests or personal relationships that could have appeared to influence the work reported in this paper.

Data availability

Data will be made available on request.

Acknowledgments

We are grateful to Professor Q. Zhang and his team of Tsinghua University who provided the gridded monthly emission inventory processed by the Multi-resolution Emission Inventory of China (MEIC model). Data acquired from http://www.meicmodel.org/.

Appendix A. Supplementary data

Supplementary data to this article can be found online at https://doi.org/10.1016/j.atmosenv.2024.120708.

References

Abbatt, J.P.D., Lee, A.K.Y., Thornton, J.A., 2012. Quantifying trace gas uptake to tropospheric aerosol: recent advances and remaining challenges. Chem. Soc. Rev. 41 (19), 6555–6581.
An, Z., Huang, R.-J., Zhang, R., Tie, X., Li, G., Cao, J., et al., 2019. Severe haze in Northern China: a synergy of anthropogenic emissions and atmospheric processes. Proc. Natl. Acad. Sci. USA 116 (18), 8657–8666.
Anenberg, S.C., Horowitz, L.W., Tong, D.Q., West, J.J., 2010. An estimate of the global burden of anthropogenic ozone and fine particulate matter on premature human mortality using atmospheric modeling. Environmental Health Perspectives 118 (9), 1189–1195.
Apte, J.S., Marshall, J.D., Cohen, A.J., Brauer, M., 2015. Addressing global mortality from ambient PM2. 5. Environmental Science & Technology 49 (13), 8057–8066.
Beelen, R., Raaschou-Nielsen, O., Stafoggia, M., Andersen, Z.J., Weinmayr, G., Hoffmann, B., et al., 2014. Effects of long-term exposure to air pollution on natural-cause mortality: an analysis of 22 European cohorts within the multicentre ESCAPE project. Lancet 383 (9919), 785–795.
Bell, M.L., McDermott, A., Zeger, S.L., Samet, J.M., Dominici, F., 2004. Ozone and short-term mortality in 95 US urban communities, 1987-2000. JAMA 292 (19), 2372–2378.
Brook, R.D., Rajagopalan, S., Pope III, C.A., Brook, J.R., Bhatnagar, A., Diez-Roux, A.V., et al., 2010. Particulate matter air pollution and cardiovascular disease: an update to the scientific statement from the American Heart Association. Circulation 121 (21), 2331–2378.
Burnett, R., Chen, H., Szyszkowicz, M., Fann, N., Hubbell, B., Pope, C.A., et al., 2018. Global estimates of mortality associated with long-term exposure to outdoor fine particulate matter. Proc. Natl. Acad. Sci. USA 115 (38), 9592–9597.
Burnett, R.T., Pope III, C.A., Ezzati, M., Olives, C., Lim, S.S., Mehta, S., et al., 2014. An integrated risk function for estimating the global burden of disease attributable to ambient fine particulate matter exposure. Environmental Health Perspectives 122 (4), 397–403.
Burns, J., Boogaard, H., Polus, S., Pfadenhauer, L.M., Rohwer, A.C., van Erp, A.M., et al., 2020. Interventions to reduce ambient air pollution and their effects on health: an abridged Cochrane systematic review. Environ. Int. 135, 105400.
Chen, H., Zhuang, B., Liu, J., Wang, T., Li, S., Xie, M., et al., 2019. Characteristics of ozone and particles in the near-surface atmosphere in the urban area of the Yangtze River Delta, China. Atmos. Chem. Phys. 19 (7), 4153–4175.
Chen, K., Wang, P., Zhao, H., Wang, P., Gao, A., Myllyvirta, L., Zhang, H., 2021. Summertime O3 and related health risks in the north China plain: a modeling study using two anthropogenic emission inventories. Atmos. Environ. 246, 118087.
Chen, M., Gong, Y., Li, Y., Lu, D., Zhang, H., 2016. Population distribution and urbanization on both sides of the Hu Huanyong Line: Answering the Premier's question. J. Geogr. Sci. 26 (11), 1593–1610.
Cohen, A.J., Brauer, M., Burnett, R., Anderson, H.R., Frostad, J., Estep, K., et al., 2017. Estimates and 25-year trends of the global burden of disease attributable to ambient air pollution: an analysis of data from the Global Burden of Diseases Study 2015. Lancet 389 (10082), 1907–1918.
Collaborators, G.2015R.F., 2016. Global, regional, and national comparative risk assessment of 79 behavioural, environmental and occupational, and metabolic risks or clusters of risks, 1990–2015: a systematic analysis for the Global Burden of Disease Study 2015. Lancet (London, England) 388 (10053), 1659.
Davis, R.A., Lii, K.-S., Politis, D.N., 2011. Remarks on some nonparametric estimates of a density function. In: Selected Works of Murray Rosenblatt. Springer, pp. 95–100.
Dehkhoda, N., Noh, Y., Joo, S., 2020. Long-term variation of black carbon absorption aerosol optical depth from AERONET data over east Asia. Rem. Sens. 12 (21), 3551.
Ding, A.J., Fu, C.B., Yang, X.Q., Sun, J.N., Zheng, L.F., Xie, Y.N., et al., 2013. Ozone and fine particle in the western Yangtze River Delta: an overview of 1 yr data at the SORPES station. Atmos. Chem. Phys. 13 (11), 5813–5830.
Fan, H., Zhao, C., Yang, Y., 2020a. A comprehensive analysis of the spatio-temporal variation of urban air pollution in China during 2014–2018. Atmos. Environ. 220, 117066.
Fan, H., Zhao, C., Ma, Z., Yang, Y., 2020b. Atmospheric inverse estimates of CO emissions from Zhengzhou, China. Environmental Pollution 267, 115164.
Fan, H., Wang, Y., Zhao, C., Yang, Y., Yang, X., Sun, Y., Jiang, S., 2021. The role of primary emission and transboundary transport in the air quality changes during and after the COVID-19 lockdown in China. Geophys. Res. Lett. 48 (7), e2020GL091065.
Feigin, V., Collaborators, G.2017R.F., 2018. Global, regional, and national comparative risk assessment of 84 behavioural, environmental and occupational, and metabolic risks or clusters of risks for 195 countries and territories, 1990–2017: a systematic analysis for the Global Burden of Disease Study 2017. Lancet 392 (10159), 1923–1994.
Feng, Y., Ning, M., Lei, Y., Sun, Y., Liu, W., Wang, J., 2019. Defending blue sky in China: effectiveness of the "air pollution prevention and control action plan" on air quality improvements from 2013 to 2017. J. Environ. Manag. 252, 109603.
Hao, Y., Balluz, L., Strosnider, H., Wen, X.J., Li, C., Qualters, J.R., 2015. Ozone, fine particulate matter, and chronic lower respiratory disease mortality in the United States. Am. J. Respir. Crit. Care Med. 192 (3), 337–341.
Hilboll, A., Richter, A., Burrows, J.P., 2013. Long-term changes of tropospheric NO2 over megacities derived from multiple satellite instruments. Atmos. Chem. Phys. 13 (8), 4145.
Hoek, G., Krishnan, R.M., Beelen, R., Peters, A., Ostro, B., Brunekreef, B., Kaufman, J.D., 2013. Long-term air pollution exposure and cardio-respiratory mortality: a review. Environmental Health 12 (1), 43.
Huang, J., Pan, X., Guo, X., Li, G., 2018. Health impact of China's Air Pollution Prevention and Control Action Plan: an analysis of national air quality monitoring and mortality data. Lancet Planet. Health 2 (7), e313–e323.
Huang, X., Ding, A., Gao, J., Zheng, B., Zhou, D., Qi, X., et al., 2020. Enhanced secondary pollution offset reduction of primary emissions during COVID-19 lockdown in China. Natl. Sci. Rev. 8 (2), nwaa137.
Jacob, D.J., 2000. Heterogeneous chemistry and tropospheric ozone. Atmos. Environ. 34 (12–14), 2131–2159.
Jerrett, M., Burnett, R.T., Pope III, C.A., Ito, K., Thurston, G., Krewski, D., et al., 2009. Long-term ozone exposure and mortality. N. Engl. J. Med. 360 (11), 1085–1095.
Krotkov, N.A., McClure, B., Dickerson, R.R., Carn, S.A., Li, C., Bhartia, P.K., et al., 2008. Validation of SO2 retrievals from the ozone monitoring instrument over NE China. J. Geophys. Res. Atmos. 113 (D16).
Kuerban, M., Waili, Y., Fan, F., Liu, Y., Qin, W., Dore, A.J., et al., 2020. Spatio-temporal patterns of air pollution in China from 2015 to 2018 and implications for health risks. Environmental Pollution 258, 113659.
Lefohn, A.S., Malley, C.S., Smith, L., Wells, B., Hazucha, M., Simon, H., et al., 2018. Tropospheric ozone assessment report: global ozone metrics for climate change, human health, and crop/ecosystem research. Elementa: Science of the Anthropocene 6.
Lelieveld, J., Barlas, C., Giannadaki, D., Pozzer, A., 2013. Model calculated global, regional and megacity premature mortality due to air pollution. Atmos. Chem. Phys. 13 (14), 7023–7037.
Li, C., McLinden, C., Fioletov, V., Krotkov, N., Carn, S., Joiner, J., et al., 2017. India is overtaking China as the world's largest emitter of anthropogenic sulfur dioxide. Sci. Rep. 7 (1), 1–7.
Li, J., Wang, Z., Wang, X., Yamaji, K., Takigawa, M., Kanaya, Y., et al., 2011. Impacts of aerosols on summertime tropospheric photolysis frequencies and photochemistry over Central Eastern China. Atmos. Environ. 45 (10), 1817–1829.
Li, K., Jacob, D.J., Liao, H., Zhu, J., Shah, V., Shen, L., et al., 2019a. A two-pollutant strategy for improving ozone and particulate air quality in China. Nat. Geosci. 12 (11), 906–910.
Li, K., Jacob, D.J., Liao, H., Shen, L., Zhang, Q., Bates, K.H., 2019b. Anthropogenic drivers of 2013–2017 trends in summer surface ozone in China. Proc. Natl. Acad. Sci. USA 116 (2), 422–427.
Li, L., Chen, B., Zhang, Y., Zhao, Y., Xian, Y., Xu, G., et al., 2018. Retrieval of daily PM2. 5 concentrations using nonlinear methods: a case study of the Beijing–Tianjin–Hebei region, China. Rem. Sens. 10 (12), 2006.
Li, M., Wang, T., Xie, M., Li, S., Zhuang, B., Chen, P., et al., 2018. Agricultural fire impacts on ozone photochemistry over the Yangtze River Delta region, East China. J. Geophys. Res. Atmos. 123 (12), 6605–6623.
Li, R., Li, Z., Gao, W., Ding, W., Xu, Q., Song, X., 2015. Diurnal, seasonal, and spatial variation of PM2. 5 in Beijing. Sci. Bull. 60 (3), 387–395.
Li, T., Zhang, Y., Wang, J., Xu, D., Yin, Z., Chen, H., et al., 2018. All-cause mortality risk associated with long-term exposure to ambient PM2· 5 in China: a cohort study. Lancet Public Health 3 (10), e470–e477.
Lu, X., Hong, J., Zhang, L., Cooper, O.R., Schultz, M.G., Xu, X., et al., 2018. Severe surface ozone pollution in China: a global perspective. Environ. Sci. Technol. Lett. 5 (8), 487–494.
Lu, X., Zhang, L., Zhao, Y., Jacob, D.J., Hu, Y., Hu, L., et al., 2019. Surface and tropospheric ozone trends in the Southern Hemisphere since 1990: possible linkages to poleward expansion of the Hadley Circulation. Sci. Bull. 64 (6), 400–409.
Luben, T.J., Buckley, B.J., Patel, M.M., Stevens, T., Coffman, E., Rappazzo, K.M., et al., 2018. A cross-disciplinary evaluation of evidence for multipollutant effects on cardiovascular disease. Environ. Res. 161, 144–152.
Maji, K.J., Ye, W.-F., Arora, M., Nagendra, S.S., 2019. Ozone pollution in Chinese cities: assessment of seasonal variation, health effects and economic burden. Environmental Pollution 247, 792–801.
Malley, C.S., Henze, D.K., Kuylenstierna, J.C., Vallack, H.W., Davila, Y., Anenberg, S.C., et al., 2017. Updated global estimates of respiratory mortality in adults$\geq$ 30 years of

age attributable to long-term ozone exposure. Environmental Health Perspectives 125 (8), 087021.
Mao, J., Fan, S., Jacob, D.J., Travis, K.R., 2013. Radical loss in the atmosphere from Cu-Fe redox coupling in aerosols. Atmos. Chem. Phys. 13 (2), 509–519.
Menon, S., Unger, N., Koch, D., Francis, J., Garrett, T., Sednev, I., et al., 2008. Aerosol climate effects and air quality impacts from 1980 to 2030. Environ. Res. Lett. 3 (2), 024004.
Murray, C.J., Ezzati, M., Lopez, A.D., Rodgers, A., Vander Hoorn, S., 2003. Comparative quantification of health risks: conceptual framework and methodological issues. Popul. Health Metrics 1 (1), 1.
Nations, U., 2018. World Population Prospect 2017.
Nawahda, A., Yamashita, K., Ohara, T., Kurokawa, J., Yamaji, K., 2012. Evaluation of premature mortality caused by exposure to PM 2.5 and ozone in East Asia: 2000, 2005, 2020. Water, Air, Soil Pollut. 223 (6), 3445–3459.
Nichols, E., Szoeke, C.E., Vollset, S.E., Abbasi, N., Abd-Allah, F., Abdela, J., et al., 2019. Global, regional, and national burden of Alzheimer's disease and other dementias, 1990–2016: a systematic analysis for the Global Burden of Disease Study 2016. Lancet Neurol. 18 (1), 88–106.
Organization, W.H., 2006. WHO Air Quality Guidelines for Particulate Matter, Ozone, Nitrogen Dioxide and Sulfur Dioxide: Global Update 2005: Summary of Risk Assessment. World Health Organization.
Real, E., Sartelet, K., 2011. Modeling of photolysis rates over Europe: impact on chemical gaseous species and aerosols. Atmos. Chem. Phys. 11 (4), 1711–1727.
Schnell, J.L., Prather, M.J., 2017. Co-occurrence of extremes in surface ozone, particulate matter, and temperature over eastern North America. Proc. Natl. Acad. Sci. USA 114 (11), 2854–2859.
Seinfeld, J.H., Pandis, S.N., 2016. Atmospheric Chemistry and Physics: from Air Pollution to Climate Change. John Wiley & Sons.
Seinfeld, J.H., Pandis, S.N., Noone, K., 1998. Atmospheric chemistry and physics: from air pollution to climate change. PhT 51 (10), 88.
Shen, H., Tao, S., Chen, Y., Ciais, P., Güneralp, B., Ru, M., et al., 2017. Urbanization-induced population migration has reduced ambient PM2. 5 concentrations in China. Sci. Adv. 3 (7), e1700300.
Silver, B., Reddington, C.L., Arnold, S.R., Spracklen, D.V., 2018. Substantial changes in air pollution across China during 2015–2017. Environ. Res. Lett. 13 (11), 114012.
Song, Y., Wang, X., Maher, B.A., Li, F., Xu, C., Liu, X., et al., 2016. The spatial-temporal characteristics and health impacts of ambient fine particulate matter in China. J. Clean. Prod. 112, 1312–1318.
Stanaway, J.D., Afshin, A., Gakidou, E., Lim, S.S., Abate, D., Abate, K.H., et al., 2018. Global, regional, and national comparative risk assessment of 84 behavioural, environmental and occupational, and metabolic risks or clusters of risks for 195 countries and territories, 1990–2017: a systematic analysis for the Global Burden of Disease Study 2017. Lancet 392 (10159), 1923–1994.
Taketani, F., Kanaya, Y., Pochanart, P., Liu, Y., Li, J., Okuzawa, K., et al., 2012. Measurement of overall uptake coefficients for HO 2 radicals by aerosol particles sampled from ambient air at Mts. Tai and Mang (China). Atmos. Chem. Phys. 12 (24), 11907–11916.
Tan, Z., Lu, K., Dong, H., Hu, M., Li, X., Liu, Y., et al., 2018. Explicit diagnosis of the local ozone production rate and the ozone-NOx-VOC sensitivities. Sci. Bull. 63 (16), 1067–1076.
Tie, X., Madronich, S., Walters, S., Edwards, D.P., Ginoux, P., Mahowald, N., et al., 2005. Assessment of the global impact of aerosols on tropospheric oxidants. J. Geophys. Res. Atmos. 110 (D3).
Wang, C., Qi, Y., Chen, Z., 2023. Explainable Gated Recurrent Unit to explore the effect of co-exposure to multiple air pollutants and meteorological conditions on mental health outcomes. Environ. Int. 171, 107689.
Wang, D., Zhou, B., Fu, Q., Zhao, Q., Zhang, Q., Chen, J., et al., 2016. Intense secondary aerosol formation due to strong atmospheric photochemical reactions in summer: observations at a rural site in eastern Yangtze River Delta of China. Sci. Total Environ. 571, 1454–1466.
Wang, P., Qiao, X., Zhang, H., 2020. Modeling PM2. 5 and O3 with aerosol feedbacks using WRF/Chem over the Sichuan Basin, southwestern China. Chemosphere 254, 126735.
Wang, Q., Wang, J., He, M.Z., Kinney, P.L., Li, T., 2018. A county-level estimate of PM2. 5 related chronic mortality risk in China based on multi-model exposure data. Environ. Int. 110, 105–112.
Wang, T., Xue, L., Brimblecombe, P., Lam, Y.F., Li, L., Zhang, L., 2017. Ozone pollution in China: a review of concentrations, meteorological influences, chemical precursors, and effects. Sci. Total Environ. 575, 1582–1596.
Wang, Y., Gao, W., Wang, S., Song, T., Gong, Z., Ji, D., et al., 2020. Contrasting trends of PM2. 5 and surface ozone concentrations in China from 2013 to 2017. Natl. Sci. Rev. 7 (8), 1331–1339.
Wu, W., Yao, M., Yang, X., Hopke, P.K., Choi, H., Qiao, X., et al., 2021. Mortality burden attributable to long-term ambient PM2. 5 exposure in China: using novel exposure-response functions with multiple exposure windows. Atmos. Environ. 246, 118098.
Xiao, Q., Geng, G., Liang, F., Wang, X., Lv, Z., Lei, Y., et al., 2020. Changes in spatial patterns of PM2. 5 pollution in China 2000–2018: impact of clean air policies. Environ. Int. 141, 105776.
Xie, M., Zhu, K., Wang, T., Chen, P., Han, Y., Li, S., et al., 2016. Temporal characterization and regional contribution to O3 and NOx at an urban and a suburban site in Nanjing, China. Sci. Total Environ. 551, 533–545.
Xie, Y., Dai, H., Zhang, Y., Wu, Y., Hanaoka, T., Masui, T., 2019. Comparison of health and economic impacts of PM2. 5 and ozone pollution in China. Environ. Int. 130, 104881.
Yue, H., He, C., Huang, Q., Yin, D., Bryan, B.A., 2020a. Stronger policy required to substantially reduce deaths from PM 2.5 pollution in China. Nat. Commun. 11 (1), 1–10.
Yue, H., He, C., Huang, Q., Yin, D., Bryan, B.A., 2020b. Stronger policy required to substantially reduce deaths from PM 2.5 pollution in China. Nat. Commun. 11 (1), 1–10.
Zhang, K., Zhao, C., Fan, H., Yang, Y., Sun, Y., 2020. Toward understanding the differences of PM2. 5 characteristics among five China urban cities. Asia-Pacific Journal of Atmospheric Sciences 56 (4), 493–502.
Zhang, Q., Zheng, Y., Tong, D., Shao, M., Wang, S., Zhang, Y., et al., 2019. Drivers of improved PM2. 5 air quality in China from 2013 to 2017. Proc. Natl. Acad. Sci. USA 116 (49), 24463–24469.
Zhao, S., Yin, D., Yu, Y., Kang, S., Qin, D., Dong, L., 2020. PM2. 5 and O3 pollution during 2015–2019 over 367 Chinese cities: spatiotemporal variations, meteorological and topographical impacts. Environmental Pollution, 114694.
Zheng, B., Tong, D., Li, M., Liu, F., Hong, C., Geng, G., et al., 2018. Trends in China's anthropogenic emissions since 2010 as the consequence of clean air actions. Atmos. Chem. Phys. 18 (19), 14095–14111.
Zhong, M., Chen, F., Saikawa, E., 2019. Sensitivity of projected PM2. 5-and O3-related health impacts to model inputs: a case study in mainland China. Environ. Int. 123, 256–264.
Zhou, M., Wang, H., Zhu, J., Chen, W., Wang, L., Liu, S., et al., 2016. Cause-specific mortality for 240 causes in China during 1990–2013: a systematic subnational analysis for the Global Burden of Disease Study 2013. Lancet 387 (10015), 251–272.
Zhou, Y., Guo, J., Wang, Z., Zhang, B., Sun, Z., Yun, X., Zhang, J., 2020. Levels and inhalation health risk of neonicotinoid insecticides in fine particulate matter (PM2. 5) in urban and rural areas of China. Environ. Int. 142, 105822.
Zhu, J., Chen, L., Liao, H., Dang, R., 2019. Correlations between PM2. 5 and ozone over China and associated underlying reasons. Atmosphere 10 (7), 352.
Zou, B., Li, S., Lin, Y., Wang, B., Cao, S., Zhao, X., et al., 2020. Efforts in reducing air pollution exposure risk in China: State versus individuals. Environ. Int. 137, 105504.
Zunt, J.R., Kassebaum, N.J., Blake, N., Glennie, L., Wright, C., Nichols, E., et al., 2018. Global, regional, and national burden of meningitis, 1990–2016: a systematic analysis for the Global Burden of Disease Study 2016. Lancet Neurol. 17 (12), 1061–1082.